
Article:
Morris, J.D., Daood, S.S. and Nimmo, W. orcid.org/0000-0001-5571-026X (2020) Agglomeration and the effect of process conditions on fluidized bed combustion of biomasses with olivine and silica sand as bed materials : pilot-scale investigation. Biomass and Bioenergy, 142. 105806. ISSN 1873-2909

https://doi.org/10.1016/j.biombioe.2020.105806

Agglomeration and the effect of process conditions on fluidized bed combustion of biomasses with olivine and silica sand as bed materials: Pilot-scale investigation

Jonathan D. Morris[a], Syed Sheraz Daood[a,b,*], William Nimmo[a]

[a] *Energy Engineering Group, Energy 2050, Department of Mechanical Engineering, University of Sheffield, Sheffield, S3 7RD, United Kingdom*

[b] *Institute of Chemical Engineering and Technology, University of the Punjab, Quaid-e-Azam Campus, Lahore, Pakistan*

** Corresponding author at: Ella Armitage Building, Energy Engineering Group, Energy 2050, Department of Mechanical Engineering, University of Sheffield, Sheffield, S3 7RD, UK; Institute of Chemical Engineering and Technology, University of the Punjab, Quaid-e-Azam Campus, Lahore, Pakistan.*

E-mail addresses: s.daood@sheffield.ac.uk; sdaood.icet@pu.edu.pk (S.S. Daood); w.nimmo@sheffield.ac.uk (W. Nimmo)

Abstract

Bubbling fluidized bed combustion of biomass has benefits of fuel flexibility, high combustion efficiency, and lower emissions. Bed agglomeration is where bed particles adhere together with alkali silicate melts and can lead to unscheduled plant shutdown. This pilot-scale study investigates performance and agglomeration when varying fuel (white wood, oat hull waste, miscanthus, wheat straw), bed height, bed material, and includes a novel spatial analysis of agglomerates from different bed locations. White wood was the best performing fuel and did not undergo bed defluidization due to its low ash content (0.5% mass), whereas wheat straw (6.67% mass ash) performed worst (defluidization times <25 minutes). Olivine was a superior bed material to silica sand, with 25%+ longer defluidization times with the worst performing fuel (wheat straw). Calcium-rich layers formed at olivine particle surfaces within wheat straw ash melts, and capillary action drew potassium silicate melt fractions into olivine particle fractures. An analysis of agglomerate samples from different bed spatial locations following tests with oat hull waste showed that ash layers on agglomerates retrieved further from the

landing point of fuel onto the bed had reduced potassium and elevated calcium, likely due to reduced availability of fresh fuel ash for reaction with bed material.

Keywords

Fluidized bed, Combustion, Biomass, Emissions, Agglomeration, Agricultural waste

Abbreviations

Ar	Archimedes number
BFB	Bubbling fluidized bed
d_p	Bed particle mean diameter (μm)
FBC	Fluidized bed combustion
IED	Industrial emissions directive
NDIR	Non-dispersive infrared sensor
Re_p	Reynolds number
SEM/EDX	Scanning electron microscopy with energy dispersive x-ray spectroscopy
t_{def}	Defluidization time (mins)
U	Fluidization velocity (m s^{-1})
U/U_{mf}	Fluidization number
U_{mf}	Minimum fluidization velocity (m s^{-1})

1. Introduction

Renewable biomass fuels are increasingly selected as a fuel source for thermal power generation, due to their positioning as a near carbon neutral alternative to fossil fuels such as coal [1]. Biomass may come in numerous forms, such as woody, agricultural, herbaceous, or biomass waste (e.g. demolition wood) fuels [2]. However, biomass fuel compositions can be highly variable, changing with factors such as source location and seasonal variation [2]. This wide variance has led to greater use of fluidized bed combustion (FBC) technology. FBC utilises a bed of suspended particles for fuel combustion, enabling use of larger or mixed fuel sizes and compositions whilst still allowing complete combustion to occur [3]. In comparison, traditional pulverized fuel boilers for biomass require consistent fuel particle sizes and compositions for near instantaneous fuel particle combustion [4]. Other technology options such as grate boilers can be competitive with FBC boilers for poorer quality biomasses, depending on the fuel and required boiler size [5].

Biomass ash still presents numerous issues, even within FBC boilers, such as corrosion, slagging and fouling, and bed agglomeration [6, 7, 8]. Bed agglomeration is the process by which bed material adheres together into agglomerates, and principally occurs via one of two mechanisms. When silica sand bed materials are used, the alkali metals in biomass ash typically react with silica in the sand to form an alkali silicate coating, in what is termed coating-induced agglomeration, and over time there is the development of two to three distinct coating layers on the bed material [9, 10, 11]. When non-silica based bed materials are used, or with fuels that have sufficient levels of both alkali metals and silica, the fuel ash itself forms an alkali silicate melt in what is widely termed melt-induced agglomeration [9, 12]. Sufficient accumulation of agglomerates within a fluidized bed will ultimately result in bed defluidization, which in the context of a commercial FBC boiler would result in an unscheduled plant outages at substantial cost to operators [13]. An example of revenue loss due to an unscheduled outage is contained within the Supplementary Data.

Many groups have investigated agglomeration behaviours with different fuels, bed materials and operational conditions, typically with smaller lab-scale fluidized bed units. Mechanisms of agglomeration with wood fuels and silica sands have received significant attention [9, 10, 11, 14, 15], along with some other agricultural fuels such as straws [16, 17, 18, 19]. Wood fuels have generally been found to perform very well with few agglomeration issues, and are frequently used in commercial fluidized bed boilers [20]. Straws have generally been found to suffer from severe melt-induced agglomeration issues, and thus are much harder to use in full-scale FBC units. Due to the broad range of biomass fuels, many fuel candidates have yet to receive equivalent levels of investigation as to their agglomeration behaviours and performance. For example the energy crop miscanthus has received much attention in the bioenergy field as a whole [21], but there are limited studies as to its potential agglomeration behaviours [22, 23, 24]. Some agricultural waste fuels, such as oat hull waste, appear to have received no attention with regards to agglomeration behaviours in prior literature. This lack of experimental study is of importance because at present, non-experimental approaches to predicting agglomeration difficulties, such as fuel/ash indices or thermochemical modelling, carry substantial levels of uncertainty [25].

Mitigation approaches to agglomeration have also been widely studied in literature, such as the use of alternative bed materials [26, 27, 28, 29] (as opposed to silica sand), additives [23, 30, 31], or optimisation of operational conditions [32, 33]. The use of the bed material olivine has been the subject of numerous studies across both fluidized bed combustion and gasification units, principally with wood fuels [26, 27, 28, 29], and has been used in commercial units [20]. In these studies, olivine was being found to be beneficial at mitigating agglomeration, as it did not react with biomass ash to form alkali silicate melts unlike silica sand. This was due to its significantly different composition as a magnesium iron silicate. Fewer agglomeration studies exist for olivine with other fuels. The study of Michel, et al. [24] with miscanthus, saw a clear difference in agglomeration behaviours versus silica sand, with the migration of iron from olivine into surrounding ash melt deposits evident.

The impact of various operational characteristics on agglomeration have also been investigated in the literature. Studies into the effect of static bed height have been limited and have shown contradictory results. The work of Lin & Wey [32] showed that increases to the static bed height resulted in decreases to defluidization time, whereas Chaivatamaset, et al. [33] observed that increased bed heights increased the defluidization time from initial fuel feeding. These contradictory studies, and the limited amount of such studies, make it difficult to draw a conclusion as to the real impact of bed height.

Whilst many studies have investigated agglomeration mechanisms through analysis of individual bed agglomerates, very few have considered the presence of any bed scale variances regarding agglomeration. The only such study in literature is that of Duan, et al. [17] where agglomerates were retrieved from three different vertical levels in a lab-scale FBC unit. Potassium levels in agglomerates from the upper bed region were observed as being higher than those from other regions. It was suggested that agglomerates were forming in this upper bed region. The prevalence of other components that can influence agglomeration (e.g. sodium, phosphorous [34, 35, 36]) were not investigated in the study, limiting conclusions. This does show a topic of interest, as an understanding of bed-scale agglomerate variances could allow for optimisation of fuel feeding arrangements in commercial boilers.

The current study thus presented an opportunity to address some of the existing gaps within the literature. Investigations have been performed on a single large pilot-scale fluidized bed combustor, as opposed to lab-scale units which are more commonly used in the literature, to increase the applicability of findings to larger scale units. In addition, it has also allowed for direct comparisons between the effects of different conditions, materials, and fuels when used in a single unit. The aims of the present study were as follows:

- Test a range of pelletized biomass fuels (white wood, oat hull waste, miscanthus, wheat straw) and investigate operational performance when using silica sand as a bed material.
- Trial use of the alternative olivine bed material (magnesium iron silicate) in comparison to silica sand.
- Initial study of the impact of static bed height and bed material particle size on the overall performance of a FBC unit.
- Investigate agglomeration mechanisms across different biomass fuels and bed materials, and determine if there is any spatial variance to agglomerate composition or structure across different regions of the bed.

2. Material and Methods

2.1. Fuels

Four pelletized woody and non-woody biomass fuels were used:

- White wood. A mixture of forestry wastes sourced from the south-eastern USA, prepared in accordance with ISO 17225–2:2014 (grade I2 industrial fuel pellet). Data on the exact species' of wood included in these wastes is not available.
- Oat hull waste (oats being *avena sativa*).
- Miscanthus (*miscanthus* × *giganteus*).
- Wheat straw (wheat being *triticum aestivum*).

These fuels were pelletized (approximate size of prepared pellets: 8mm diameter, 40mm length) and supplied by a UK biomass power generation company. Further specific details cannot be listed due to commercial confidentiality reasons. The fuels were selected as they represent a broad selection across biomass fuel types: woods, energy crops, and agricultural wastes [2]. Moreover, wood fuels are typical of commercial FBC

units [20], though there is ever present interest in widening the viable fuel envelope to cheaper agricultural fuels such as those tested here. Proximate and ultimate analyses, together with ash composition, are listed for each fuel in Table 1. Ash composition of the fuels had been previously determined by ashing of samples at 550°C followed by X-ray fluorescence spectroscopy (XRF) using an Thermo ARL Advant XP sequential X-ray fluorescence spectrometer, using a method as described in the work of Xing, et al. [37].

Table 1: Composition and properties of the four biomass fuels used in the test campaign.

Property	**White Wood Pellets**	**Oat Hull Waste Pellets**	**Miscanthus Pellets**	**Wheat Straw Pellets**
Proximate analysis (mass fraction as %; as received basis)				
Fixed carbon	16.95	15.96	16.67	17.82
Volatiles	76.70	72.56	70.56	68.38
Moisture	5.82	8.83	6.76	7.12
Ash	0.50	2.66	6.01	6.67
Gross calorific value (GCV) (MJ kg^{-1})	18.04	17.24	17.70	16.05
Ultimate analysis (mass fraction as %; as received basis)				
Carbon	47.1	42.7	42.8	40.5
Hydrogen	5.4	5.3	4.9	4.8
Oxygen (by difference)	40.9	39.4	38.9	40.0
Nitrogen	0.2	1.1	0.6	0.9
Sulphur	<0.1	<0.1	<0.1	<0.1
Moisture	5.8	8.8	6.7	7.1
Ash	0.7	2.6	6.0	6.6
Ash composition (mass fraction as % of total ash)				
SiO_2	39.8	56.0	56.5	38.4
K_2O	9.6	20.6	11.7	19.8
P_2O_5	2.2	7.9	3.9	4.8
MgO	6.3	4.8	3.2	3.6
CaO	22.7	3.9	13.5	21.1
Al_2O_3	7.5	0.8	1.4	1.6
Na_2O	6.6	1.7	3.0	6.3
Fe_2O_3	4.3	0.9	2.6	1.0
MnO	1.7	0.2	0.1	0.1
TiO_2	0.5	0.1	0.1	0.3

2.2. Bed Materials

Compositions and property data for the different types and grades of bed material used in this study are given in Table 2. The two silica sand bed materials were supplied by Universal Mineral Supplies (UMS) Ltd. The two olivine bed materials were supplied by LKAB Minerals Ltd. Silica sand was chosen as it reflects a low-cost baseline bed material for commercial FBC boilers. Olivine is a more expensive option that has been proven to be effective with woody fuels, including use in commercial boilers [20], but there are fewer works investigating use of olivine with non-woody fuels as was performed here.

Table 2: Composition and property data for the bed materials used in the test campaign.

Property	**Sand 'A'**	**Sand 'B'**	**Olivine 'A'**	**Olivine 'B'**
Physical properties				
Particle mean diameter (μm)	639	853	536	664
Min. particle diameter (μm)	355	500	125	106
Max. particle diameter (μm)	1180	1180	1000	1400
Bulk density (kg m^{-3})	1639	1600	1700-1900	1600-1900
Particle density (kg m^{-3})	2650[a]	2650	3300	3300
Hardness (Mohs)		6.0-7.0	6.5-7.0	6.5-7.0
Composition (mass fraction as %)				
SiO_2	97.15	97.00-99.80	41.58	42.06
Fe_2O_3	1.96	1.00-1.50	7.21	7.13
Al_2O_3	0.28	0.50-1.50	0.41	1.13
CaO		<0.20	0.06	0.45
MgO		<0.20	50.03	46.83
TiO_2	0.01	<0.20		
K_2O	0.05			0.07
Na_2O	<0.05			
Cr_2O_3			0.19	0.44
Mn_3O_4			0.10	0.10
ZrO_2				0.06
Loss on ignition	0.44	Max. 3.00	Max. 2.00	Max. 2.00

[a] *Assumed to be same particle density as sand 'B'.*

2.3. Pilot-Scale Fluidized Bed Combustor

A pilot-scale bubbling fluidized bed (BFB) combustor has been used to perform all combustion trials. A simplified process flow diagram of the unit is given in Figure 1. This unit is equipped with various temperature, pressure and emissions monitoring capabilities. Fuel is fed from a hopper via a screw feeder onto the top of the bed surface in the combustion chamber, as is seen frequently in commercial BFB boilers [38]. Within the combustion chamber, seven thermocouples are present in the bed and above bed region, with three others present through the freeboard region. The pressure drop across the bed and absolute pressure in the freeboard are measured via static pressure probes connected to pressure transducers. Emissions are measured from a flue gas sample line inserted after the cyclone separator. Flue gas in this sample line passes through several filtering and moisture removal stages and is then split into three streams to enter one of:

- A Fuji Electric "ZRE" single beam non-dispersive infrared sensor (NDIR) gas analyser, for measurement of NO (ppm), SO_2 (ppmv), and CO_2 (vol.%) content.
- A Fuji Electric "ZKG" dual beam NDIR gas analyser, for measurement of measurement of SO_2 (vol.%), CO (ppmv), and O_2 (vol.%) content.
- A Signal NO_x Series 440 (Model 443) chemiluminescence NO_x analyser, for measurement of NO (ppmv) or NO_x (ppmv) content.

Gas analysers were calibrated with calibration gas cylinders to ensure their accuracy. The ZRE and ZKJ analysers have a repeatability value of ±0.5% as per the manufacturer specification. The NO_x analyser has a repeatability value of ±1% as per the manufacturer specification.

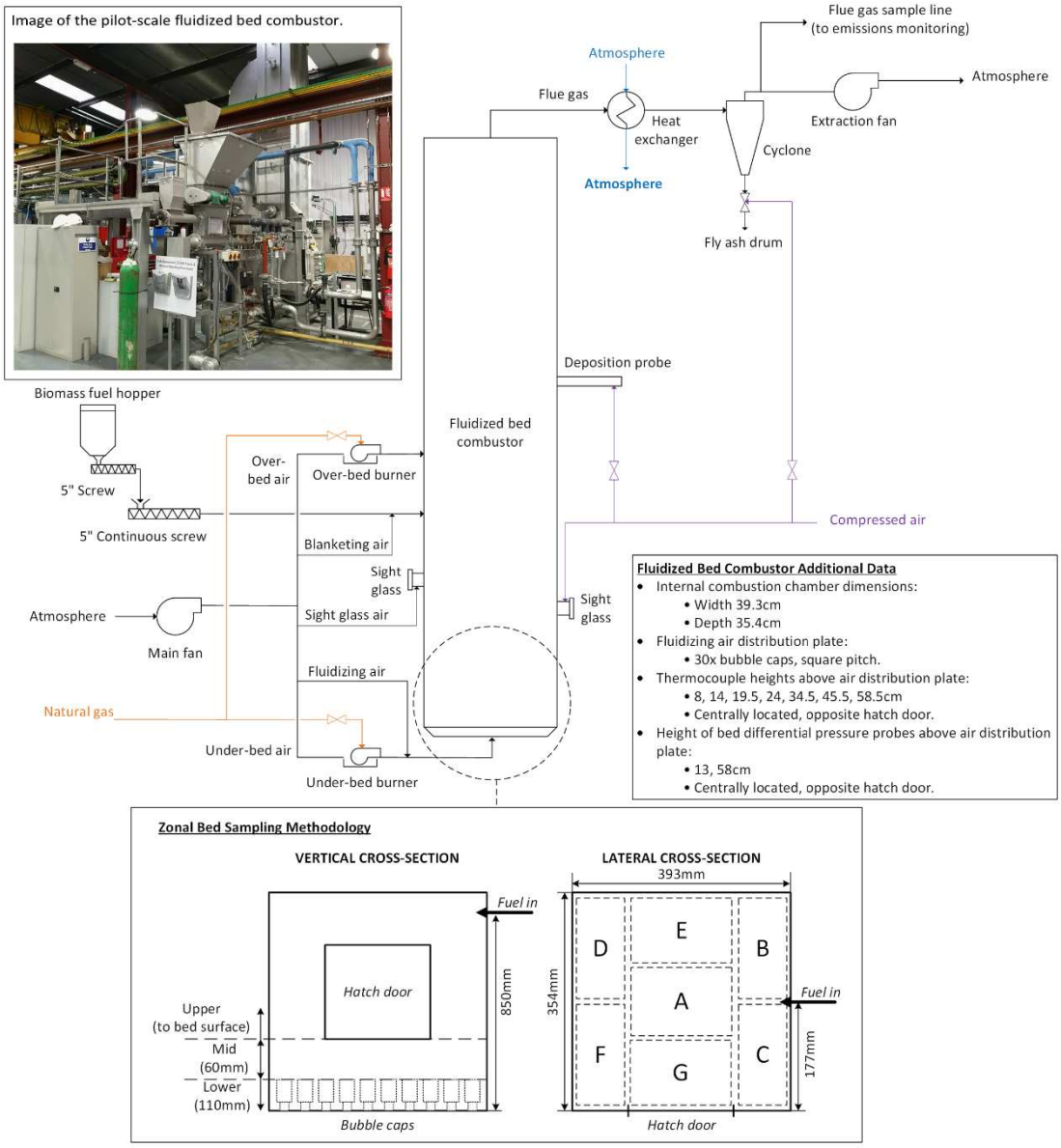

Figure 1: Process flow diagram for the pilot-scale fluidized bed combustor. Inset (top left): image of the FBC unit. Inset (bottom): diagram showing division of combustion chamber bed into seven lateral zones (A-G) and three vertical zones (lower, mid, upper) for agglomerate sample retrieval. (Not drawn to scale).

2.4. Pilot-Scale Fluidized Bed Experimental Procedure

The pilot-scale unit has been operated at a thermal rating of 50-65kW in the present campaign. Prior to each test, fresh, unused bed material was added to the unit in amounts sufficient to meet the required static bed height. During testing, the bed was first heated to 700°C+ by use of the start-up natural gas burners (labelled under-bed and over-bed burner on Figure 1). During this process, the bed was fluidized due to the heating of the bed and incoming air. Once the desired bed temperature was reached, the start-up gas burners were disabled and biomass fuel feeding was started. Air flow rates were modulated during this changeover to match the desired fluidization number for the test: the ratio of fluidizing air velocity to the minimum fluidization velocity (U/U_{mf}). The FBC unit was then allowed time to reach a steady state. Operational data was recorded continuously, with the test terminating when the bed defluidized. The defluidization time was defined as the time from initial biomass fuel feeding to the point when the bed defluidized, as defined in several other works [12, 39, 33]. Defluidization time was recorded after each test and used as a point of comparison between conditions. For the purposes of reporting, operational data was time averaged over periods typically in excess of 15 minutes, during steady-state operation on biomass. This time averaging of data was done to mitigate against any instantaneous measurement errors (e.g. to temperature, pressures, or emissions), or irregularities to fuel combustion.

Fuel input (thermal rating), static bed height and fluidization number (U/U_{mf}) were varied from 50-65kW, 19-41cm, and 2.0-3.0 respectively, with exact conditions for each test discussion in the subsequent operational results sections (3.1-3.2). Thermal rating and fluidization number were varied to achieve bed temperatures representative of a commercial BFB boiler (800-900°C), with the focus of this study being bed agglomeration. Fluidizing air input was varied from 2-3x the minimum fluidization velocity as this range was observed to create a well-mixed bubbling fluidization regime in the unit. The static bed height variance from 19-41cm reflected the lower and upper limits of the rig. Moving beyond 41cm prevented effective start up and heating of the FBC unit. At the low end, a 19cm bed height reflected a shallow bed, as approximately 7cm of this 19cm height was occupied by the bubble caps that delivered fluidizing air.

Bed samples were retrieved from the bed in a zonal manner as shown in Figure 1 after each test. A sample was taken from each of the seven (A-G) lateral zones across the "upper" and "mid" vertical strata, plus a single collection of samples that constituted the "lower" vertical strata, for a total of 15 sampling zones. Due to the proximity of bubble caps to each other, a full zonal sampling in the lower vertical strata was not viable.

2.5. SEM/EDX

Bed agglomerate samples were mounted in epoxy resin, cross-sectioned, polished and carbon coated to enable imaging and compositional analysis via scanning electron microscopy with energy dispersive x-ray spectroscopy (SEM/EDX). Analyses were performed using a ZEISS Evo MA-15 scanning electron microscope, fitted with an Oxford Instruments X-Max EDX detector, or alternatively, a FEI Inspect 50 SEM also fitted with an Oxford Instruments X-Max EDX detector. For quantitative EDX analysis, upwards of four locations or features of interest (e.g. coated particle, ash conjoined particles) were chosen per sample. An EDX point or area analysis was then performed at upwards of three areas, for each of these locations or features of interest. This measurement regime, and the subsequent use of the average of many EDX measurements in analysis and discussion, was in part to mitigate against the inherent inaccuracy of semi-qualitative and semi-quantitative EDX analysis [40, pp. 427-433].

3. Results and Discussion

3.1. Fuel Variation

3.1.1. Defluidization Time

Table 3 summarises operational data obtained from using each of the four biomass fuels with sand 'B' at consistent operational conditions, as well as olivine 'B' with wheat straw at reduced thermal rating and increased fluidization number. From the data on defluidization time, t_{def}, it is evident that white wood performs best out of the four fuels with regards to agglomeration, as it did not undergo bed defluidization, unlike the other fuels. This is likely due to the white wood having by far the lowest ash content of the fuels tested (0.5%), of which the alkali metals K_2O + Na_2O account for just 16.2% of the white wood ash. This is equivalent to the alkali metals accounting for 0.081% of the white wood. In comparison, oat hull waste had the second lowest K_2O + Na_2O content, accounting for 22.3% of a 2.66% ash content, or 0.59% of the oat hull waste. Both K_2O

and Na_2O contents are integral for formation of alkali silicate melts [10, 41]. This lack of defluidization, and favourable ash characteristics, highlights why woody fuels are generally preferred by commercial FBC boiler operators [20].

Oat hull waste and miscanthus both produced moderate t_{def} values, with miscanthus performing better than oat hull waste. These fuels have upwards of 4x the ash content of white wood, with the alkali metal content of this ash content similar or greater than that of the white wood (Table 1), thereby resulting in them having higher alkali metal contents as a proportion of the fuel as a whole. This would naturally lead to more severe agglomeration issues than with white wood. The oat hull waste used does have lower ash propensities content than miscanthus, but it also has elevated K_2O, a far lower quantity of CaO (3.9% vs. 13.5% in miscanthus ash), and slightly reduced Al_2O_3. Both calcium and aluminium-oxide based additives are known to create stable high melting point ash mixtures [30], hence a deficit of these likely led to poorer performance here.

Wheat straw, the worst performing fuel, has the highest ash content and combined K_2O + Na_2O contents of the four fuels, hence its poor t_{def} value. This is comparable to the results of others with wheat straws. For example, Yu, et al. [16] and Lin, et al. [18] saw defluidization times between 40-80 minutes and 17-45 minutes respectively, with higher times only achieved by maintaining bed temperatures at or below 800°C. This would naturally restrict the formation of molten alkali silicates, with initial melting of these occurring at around 750°C [14], at which point melting of alkali silicates would be restricted. Both groups did however use smaller lab-scale units, with each using differing operational conditions (fluidizing gas velocities, bed particle sizes), which limits the ability to draw strict quantitative comparisons. Wheat straw did perform substantially better with olivine ‘B’. However, this test was also at a significantly reduced thermal rating and increased fluidization number, both factors known to lengthen defluidization times [8]. Moreover, the olivine is of a different chemical composition (magnesium iron silicate) than sand ‘B’ (silica sand), which is known to be less reactive with biomass ash and to mitigate against agglomeration from the work of others [26, 29]. The results of an experimental comparison between the two bed materials at identical operational conditions are discussed in section 3.2.

As a whole, these defluidization time results suggest that wheat straw in particular is not a suitable fuel for FBC units due to its severe agglomeration issues. It may have some viability as a minor blend component with a woody fuel for example, with others having experimentally investigated such blends with success [31]. Conversely, the oat hull waste and miscanthus tested here, which both performed significantly better than wheat straw though still resulted in bed defluidization, may be candidates for a more significant blend fraction with a wood fuel.

Table 3: Summary of defluidization time, temperature profile and emissions data for the four fuels tested with sand 'B', and for wheat straw with olivine 'B'.

Measurement		**Sand 'B', h_{bed} 24cm, 2U/U_{mf}, 65kW Archimedes number (Ar) = 2676. Reynolds number (Re_p) = 1.86**				**Olivine 'B', h_{bed} 24cm, 2.6U/U_{mf}, 50kW Ar = 1338. Re_p = 0.96**
		White Wood	**Oat Hull Waste**	**Miscanthus**	**Wheat Straw**	**Wheat Straw**
Defluidization time from initial fuel feed (mins)		295[a]	112	159	22	114
Temperature profile (height from base of air distribution plate)	T_1 (8.0cm) (°C)		817	757	782	668
	T_2 (14.0cm) (°C)	869	822	795	825	883
	T_3 (19.5cm) (°C)	893	826	813	827	886
	T_4 (24.0cm) (°C)	897	831	825	827	879
	T_5 (34.5cm) (°C)	1005	945	933	937	968
	T_6 (45.5cm) (°C)	901		850	828	839
	T_7 (58.5cm) (°C)	861	774	789	791	755
Emissions (at 6vol.% O_2)	CO_2 (mg m^{-3}, dry)	223171	231026	216548	220398	177852
	CO (mg m^{-3}, dry)	387.98	528.00	556.86	580.52	521.37
	NO (mg m^{-3}, dry)	39.56	329.09	248.90	242.43	134.31
	NO_2 (mg m^{-3}, dry)	116.93	301.96	129.06	169.65	119.07
	NO_x (mg m^{-3}, dry)	156.49	631.04	377.95	412.08	535.37

[a] White wood did not undergo bed defluidization during the test period.

3.1.2. Temperature Profile

Temperature data in Table 3 shows that oat hull waste, miscanthus, and wheat straw all produce a very similar profile, with dense bed temperatures ranging from 750-830°C, and a peak in temperatures at the T_5 thermocouple in the above bed region (34.5cm above the air distribution plate). Note again that h_{bed} for all tests was 24cm. This profile of consistent bed temperatures and a higher temperature region above the bed is also seen in commercial BFBs [42]. Use of wheat straw with olivine 'B' instead of sand 'B' produced a slightly higher temperature profile through T_2-T_6, though conversely slightly lower temperatures in T_1 and T_7. This would suggest a slightly mixing regime, likely due to the lower particle size of olivine 'B', increased fluidization number and reduced agglomeration issues. White wood produced higher temperatures across the entire temperature profile range. A likely reason for this is the far higher volatiles content of white wood, 5%+ higher than the other fuels, allowing for greater amounts of combustion in the upper and above bed regions. A generally high temperature profile with wood fuels was seen in the work of Ribeiro, et al. [43], who tested several woody fuels in a fluidized bed combustor and saw temperatures in the high 800-low 900°C range through the bed region, and up to 1100°C in the freeboard region due to use of secondary air injection. This is comparable to the temperatures seen in Table 3 for white wood. Ribeiro, et al. [43] also cite high volatiles content of woody fuels causing an elevated temperature profile.

3.1.3. Emissions

Table 3 also shows emission data at 6vol.% O_2 for each of the fuels. NO_x emissions increased from fuel to fuel in the same order by which their fuel bound nitrogen contents increase (Table 1). This would indicate that fuel NO_x mechanisms are likely the key NO_x formation mechanism, especially when considering that temperatures within the combustor were far below the temperature at which thermal NO_x mechanisms become significant (around 1300°C) [44]. For oat hull waste, NO_x emissions were high at 631.04mg m^{-3}. NO_x emissions when combusting cereal fuels have been noted to be high in the works of others. Keppel, et al. [45] combusted oats and observed high NO_x emissions of a similar magnitude to those seen here (630mg m^{-3} on a 6vol.% O_2 basis), albeit their fuel had a higher fuel nitrogen content (1.8wt.%, as opposed to 1.1% for the oat hull waste fuel used here). With a wood fuel containing minimal fuel nitrogen

content, Keppel, et al. [45] saw NO_x emissions around 20% of those produced with oats, a similar proportional difference as seen here between the white wood and oat hull waste. This again highlights the importance of fuel nitrogen content and fuel NO_x mechanisms for NO_x formation at these sub-1000°C combustion temperatures. NO_x emissions with olivine 'B' and wheat straw were higher than those with sand 'B', though it should again be noted that tests with wheat straw and sand 'B' did not reach a steady state, and that the two tests were are differing operating conditions. The EU industrial emissions directive (IED) quotes NO_x emission limits for large biomass combustion plants from 50MW to 300MW (thermal) of 300mg m^{-3} to 200mg m^{-3} (limits decreasing with increasing thermal input) [46]. Of the four fuels tested, only white wood would meet these limits if used with sand in a large combustion plant. The pilot-scale FBC unit does not use NO_x mitigation strategies such as air staging or selective non-catalytic reduction which are known to be effective in the context of a FBC boiler [47, 48], therefore these would have to be employed when using any of the non-woody fuels tested here.

CO_2 data in Table 3 for all fuels was near identical across the four fuels with sand 'B', albeit slightly lower for olivine 'B' and wheat straw with lower thermal rating. More variation is apparent CO emissions, with white wood producing the lowest value at just under 400mg m^{-3}, whereas the other three fuels produced consistent values in the 528-580mg m^{-3} range. This may be due to the higher above bed temperatures when using white wood as discussed previously, improving burnout of any entrained carbon fines. Additionally, in the work of Ribeiro, et al. [43], two of the three woody biomasses used produced CO emissions that oscillated over a 200-800cm^3 m^{-3} range, which again compares favourably when converted with the average seen here for white wood of 387.98mg m^{-3}. Use of wheat straw with olivine, instead of sand, led to a 10% reduction in CO emissions. The work of Meng, et al. [49] tested several differently prepared types of olivine against silica sand in a fluidized bed gasifier, and observed a 5-18% reduction in CO levels when switching from silica sand to olivine due to the olivine acting as an oxygen carrier, which is a similar proportional change to that seen here under a combustion environment.

3.2. Effect of Bed Material & Height Variation on Defluidization Time

Table 4 summarises defluidization time data when varying bed material and bed height at consistent operational conditions. Bed material was varied when using the worst of the four biomass fuels tested, wheat straw. When using olivine 'B' instead of sand 'A', both of a similar particle mean diameter, d_p, of around 650µm, defluidization time was increased by around 25% when moving to olivine. This is due to the significantly different composition of the olivine in comparison to sand (see Table 2). The olivine has around 45wt.% less SiO_2 than sand and is a magnesium iron silicate material, therefore is far less reactive with alkali metals in biomass ash, a behaviour identified in the works of others such as Grimm, et al. [26], however no quantification was given as to the performance improvement when moving from silica sand to olivine in these works. As discussed in section 3.1.1, whilst this is a significant improvement when using olivine with wheat straw, switching from silica sand to an olivine bed material is still unlikely to make wheat straw a viable fuel for single fuels FBC operation due to its severe agglomeration issues.

Use of the fine size grade olivine 'A' (d_p 536µm) led to a further increase to defluidization time of around 10%. This would indicate that smaller particle size is also beneficial for lengthening the defluidization time, and is in agreement with the observation of others who reported a trend of longer defluidization times with a smaller bed particle sizes [18, 33, 16]. Here, however, it has been shown to be the case with olivine as opposed to silica sand in the other works. The likely reason for this behaviour relates to the difference in void size between larger and smaller bed particles, with the larger particles having larger voids between the particles, thus forming larger bubbles in the bed [50]. Instead of smaller dispersed bubbles through the bed, these larger bubbles rise through the bed and coalesce together, further increasing in size. The net effect of this larger particle size would be less consistent and poorer mixing patterns in the bed, allowing agglomeration to propagate more easily in these zones of poorer mixing, thus causing reduced t_{def}.

Table 4: Table summarising the effect of variation to static bed height (h_{bed}) and bed material on defluidization time (t_{def}).

Variable		Defluidization time from initial fuel feed (mins)	
		Oat Hull Waste	Wheat Straw
Bed material (conditions: h_{bed} 24cm, 3U/U_{mf}, 50kW)	Sand 'A' (639µm)[a]		131
	Olivine 'A' (536µm)[b]		177
	Olivine 'B' (664µm)[c]		164
Bed height (conditions: sand 'A', 3U/U_{mf}, 50kW)[d]	19cm	109	
	24cm	161	131
	29cm	122	118
	41cm		87

[a] *Ar = 1127. Re_p = 0.81.* [b] *Ar = 706. Re_p = 0.52.* [c] *Ar = 1338. Re_p = 0.96.* [d] *Ar = 1127. Re_p = 0.81*

Several different bed heights were tested for oat hull waste and wheat straw at identical operational conditions, and their defluidization times are shown in Table 4. For both fuels, a h_{bed} value of 24cm produced the longest t_{def}. In the case of oat hull waste, both smaller and larger bed heights produced lower t_{def} values, whilst for wheat straw incrementing beyond a 24cm static bed height also resulted in reduced defluidization times. This would imply that the optimum bed height for this FBC unit is 24cm. It should be noted that the test conditions here were different to those in the baseline fuel comparison tests of section 3.1, with considerably lower thermal ratings and higher fluidizing gas velocities, which are known to be beneficial in mitigating against agglomeration to an extent. In the case of the oat hull waste test at 19cm however, the defluidization time was very similar to that presented in Table 3 under the less favourable operating conditions. Dense bed temperatures during the 19cm bed height test with oat hull waste (Table 4) were recorded as an average of 905°C, versus an average of 826°C in the T_2-T_4 region as shown in Table 3. Elevated temperatures are known to exacerbate ash melting and agglomeration issues from numerous prior studies [18, 16], therefore are likely in part the reason for this poorer performance even with more favourable operational conditions as a whole.

These changes to defluidization time with variation to bed height are likely due to differences in bed mixing behaviours with bed height changes. A deeper bed will have poorer vertical mixing of fuel and bed material due to greater coalescence of bubbles through the bed height, allowing for bed hot spots to develop and easier formation of agglomerates. A shallower bed will have a smaller volume of bed material onto which

the same fixed thermal input of fuel is burned, increasing the ash to bed ratio, therefore, making it easier for a sufficient amount of agglomerates to accumulate and defluidize the bed. Others have produced conflicting results on the effect of bed height on defluidization time in the past [32, 33], therefore it is possible that they were only seeing one part of this trend of an optimum bed height at a fixed set of operational conditions. This would suggest that there may be room for existing FBC units to optimise their operating bed height to mitigate against agglomeration. It would also suggest that there may be an underlying relationship or correlation to determine this optimum bed height. The authors did attempt to investigate this, by comparing the current data against that available in literature [32, 33]. However, the general sparsity of literature data and wide variety of fuels, equipment scales, and operational conditions made this inconclusive. Whilst the results here are still limited, bed height may be an area of interest for continued study.

3.3. SEM/EDX

3.3.1. Structural Variation with Fuel & Bed Material

Agglomerates when using white wood and sand 'A' were seen to comprise of bed particles with thin ash coating layers of a similar thickness (<10µm) across the entire perimeter of a bed particle, and appeared to have arisen due to a coating-induced agglomeration mechanism seen in the literature whereby alkali metals in ash begin an inward reaction with silica in the bed particle [14, 15]. An example is shown in Figure 2a. Joins between coated bed particles were generally thicker than the coating layers at around 10-40µm, possibly due to molten ash deposition assisting in the formation of an agglomerate.

Use of oat hull waste with sand 'A' generally produced agglomerates of a similar structure to those seen with white wood, with an example given in Figure 2b. Observations included a thin ash coating layer around the entire perimeter of a bed particle typical of coating-induced agglomeration, thicker necks where particles were conjoined, and regions of deep ash veins and intrusions evident of the inward reaction of ash with the bed particle, or localised ash deposition.

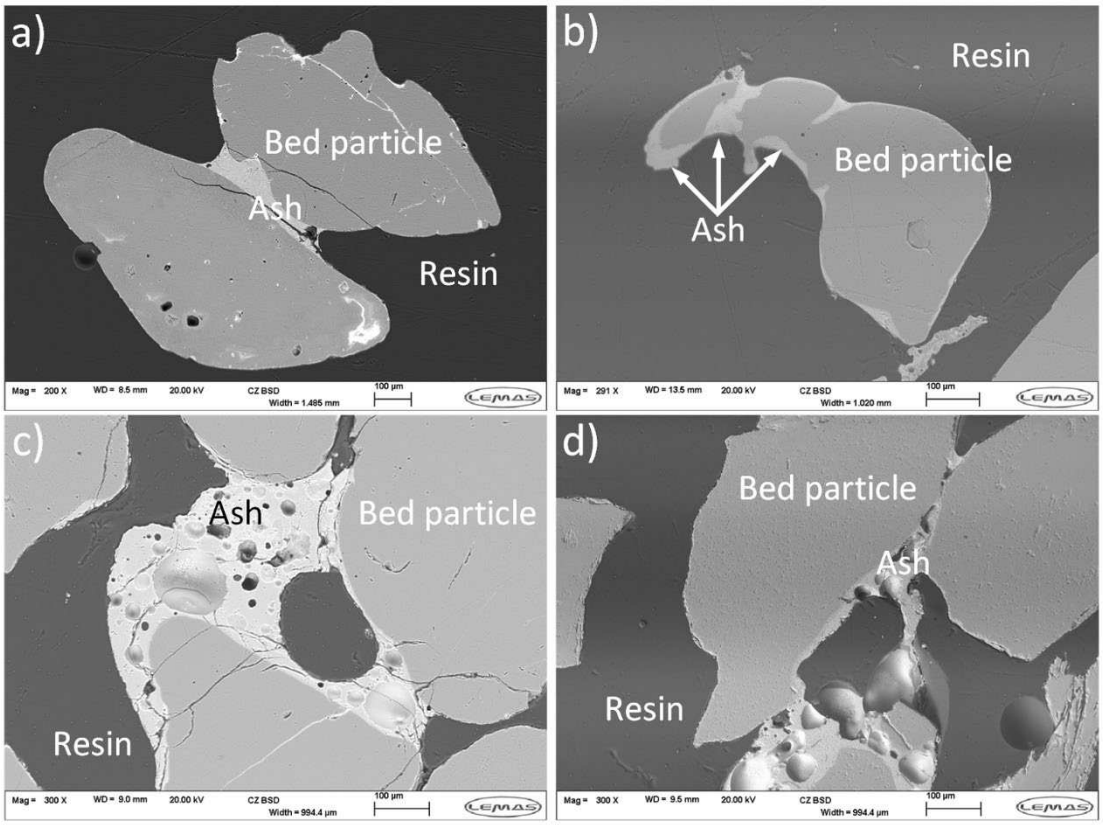

Figure 2: Backscatter SEM images showing agglomeration phenomena observed with different fuels and bed materials. a) Agglomerate from a test with white wood and sand 'A' showing a join between two sand particles, each particle with a thin <5µm ash coating layer around their perimeter. b) Coated bed particle from a test with oat hull waste and sand 'A'. A thin coating layer is evident across the entire perimeter of the particle, with some regions of increased ash deposition and reaction causing localised thicker ash layers. c) Large melt-induced agglomerate structure from a wheat straw and sand 'A' test. d) Similar large melt-induced agglomerate structure observed following a wheat straw and olivine 'B' test.

Wheat straw and sand 'A' agglomerates differed substantially in structure to those of white wood and oat hull waste, as is evident from Figure 2c. Large ash deposit phases acted as a glue holding bed particles together, with resultant bed particle joins frequently upwards of 50µm in width. There was some evidence of very thin coating layers developing on bed particle perimeters (<3µm) which can be seen on the perimeters of some of the particles in Figure 2c. This lack of coating development may be due to the shorter defluidization times seen with wheat straw in comparison to the other fuels, as discussed in section 3.1.1. Agglomeration appears to have proceeded through a melt-induced mechanism, whereby ash forms melts that then act to adhere bed material together at discontinuous locations [18, 19, 16]. Figure 2d shows example

agglomerate when using olivine 'B' with wheat straw, instead of sand 'A'. Once again, large, discontinuous, ash deposits appeared to be the predominant form of agglomeration, again indicating melt-induced agglomeration to be the agglomerate formation mechanism. No evidence could be seen for the development of ash coating layers across the entire perimeter of bed particles as would be typical for coating-induced agglomeration.

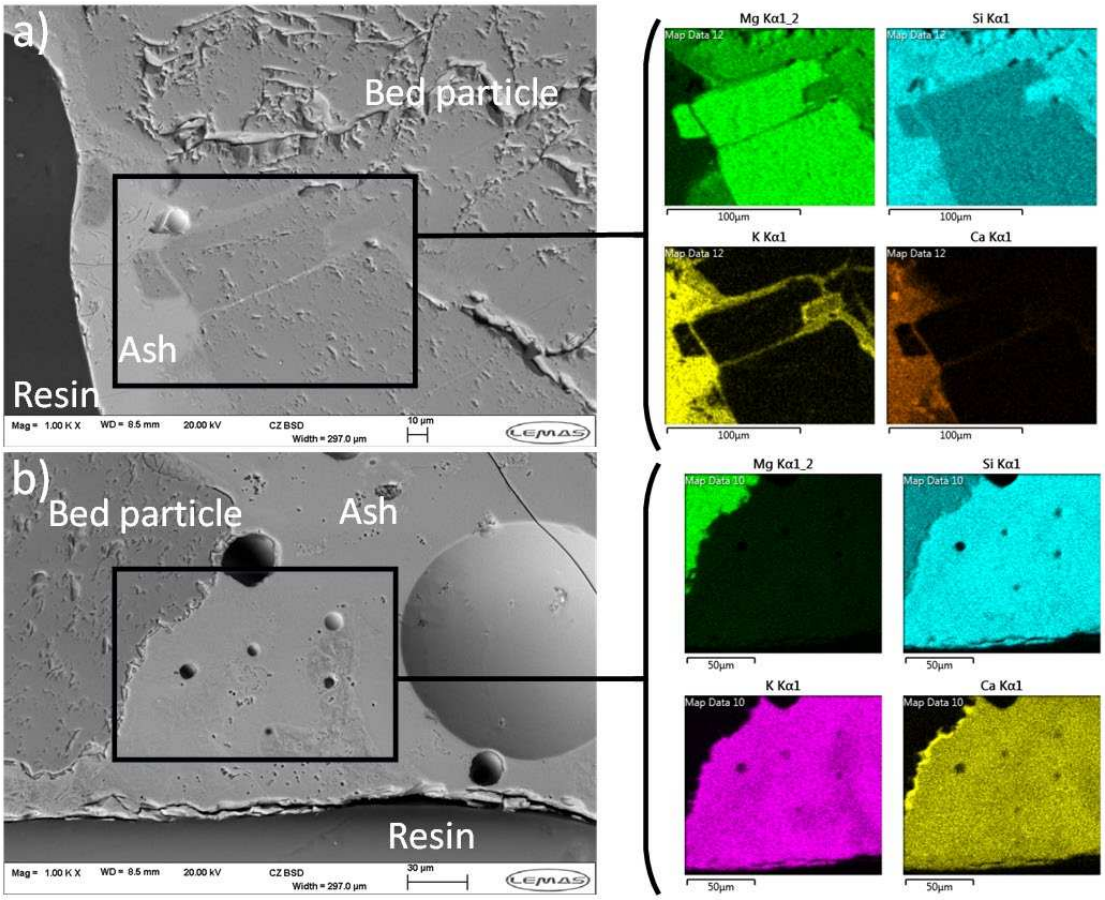

Figure 3: Backscatter SEM images & EDX mapping analysis of ash coated bed particles from wheat straw and olivine tests. Conditions: olivine 'A', 24cm bed height, 50kWth. a) Region of an olivine bed particle with several cracks/fractures. The accompanying EDX mapping analysis shows the far greater difference in potassium abundance in the outer ash deposition layer and fracture region, versus calcium abundance in the outer layer and fracture region. b) Example of the calcium-rich layers found on the surface of olivine bed particles that were embedded in large ash melt phases.

Some unique agglomeration phenomena were noted when using wheat straw and olivine 'B'. Cracked or fractured olivine bed particles were observed across numerous samples, with an example shown in Figure 3a. As is evident from the EDX mapping analysis in

Figure 3a, the potassium component, in the form of a potassium silicate melt, has fully penetrated the fracture region, and is present within this fracture region in similar abundance as is seen in the outer ash deposit layer. Calcium, however, is present mostly in the outer ash layer, with little to none present in the fracture region. Others have observed inward migration of potassium into bed material fractures and cracks in the context of silica sand with woody fuels, where it is speculated that capillary action draws the ash melt inwards [41], or that the ash melt reacts with the bed particle in fracture regions to work its way inwards [11]. As the olivine is not as reactive with biomass ash as sand is, it is more likely that the potassium silicate melt fraction has migrated into the fracture via physical means such as capillary action. This is supported by fundamental studies at elevated temperatures (1000°C+) that, when compared, show K_2O-SiO_2 melt systems [51] to have surface tension values that are over 50% less than those of CaO-SiO_2 melt systems [52] at equivalent conditions. This reduced surface tension would therefore increase capillary action and uptake of the potassium silicate melt fraction.

In regions where there was a bulk ash melt phase with embedded olivine bed particles, there was frequently the occurrence of a calcium-rich layer at the bed particle surface. An example of this is shown in Figure 3b together with an EDX mapping analysis. It is apparent from Figure 3b that this calcium-rich layer appears to be in the form of calcium crystals, though these crystals may have formed during ash cooling. Elled, et al. [53] similarly observed the formation of calcium crystals in some agglomerates from tests using a wood-straw fuel blend when using a silica sand bed, though did not suggest a reasoning. Regardless, calcium is clearly driven from the bulk ash melt phase to the bed particle surface to form this calcium-rich layer. Others have observed this formation of a calcium-rich layer when using olivine in different contexts, such as fluidized bed gasification of wood [27, 29, 28], miscanthus [22], or fluidized bed combustion of wood [26]. These other groups generally observed calcium layers to arise as a standalone feature on olivine particles, whereas here they were only observed on bed particles embedded in a large ash melt phase. This could be due to the wheat straw fuel used here as opposed to the woody fuels used in other works. The differences in the scale of the present and other studies could also partly be a dictating factor in some of the differences observed, with other studies using industrial units with operational times

upwards of dozens of hours [29]. The work of Kuba, et al. [29] presents a complete mechanism by which these calcium rich layers form with olivine. Kuba, et al. [29] proposed that calcium layering with olivine arises due to the ion substitution of Ca^{2+} into the outer olivine structure in place of either Mg^{2+} and $Fe^{2+/3+}$, with preference given to substitution of iron. The substituted magnesium or iron components are expelled from the olivine as oxides, hence the creation of a calcium rich outer layer. An elemental analysis of the ash melt surrounding olivine particles (discussed subsequently in section 3.3.2) highlights elevated magnesium and iron levels, and reduced calcium levels. This suggests that the mechanism proposed for wood fuels and olivine proposed by Kuba, et al. [29] has occurred here with wheat straw, with a movement of calcium out of the ash and into the outer olivine particle surface accompanied by expulsion of iron and magnesium into the ash melt surrounding olivine.

No works could be found in the literature analysing agglomerated olivine bed material from large commercial scale fluidized bed combustion boilers when using wheat straw or with other more common fuels such as wood, limiting the ability to compare against results from larger scale units. The works of the Kuba, et al. [29], Kirnbauer & Hofbauer [28] and others that study an industrial dual-fluidized bed gasifier using olivine and wood are perhaps the closest parallel and have been used for comparison here. This does highlight the need for further detailed studies of olivine material from commercial fluidized bed combustion boilers to confirm agglomeration behaviours.

3.3.2. Compositional Variation with Fuel & Bed Material

Figure 4 shows EDX data for ash layers on bed particles when using white wood, oat hull waste and wheat straw with sand ‘A’, and wheat straw with olivine ‘A’. Across all the data, some components presented large spreads in their composition data, represented with the 95% confidence interval bars, indicating that despite the often homogenous appearance of the ash layers, they could frequently be quite heterogeneous with regards to some chemical components. This would indicate that the exposure times of bed material here (up to around 5 hours with white wood) were not long enough to produce the chemically homogenous coating layers often seen in works that used samples from industrial boilers [9, 11] after exposure times upwards of 1-2 days.

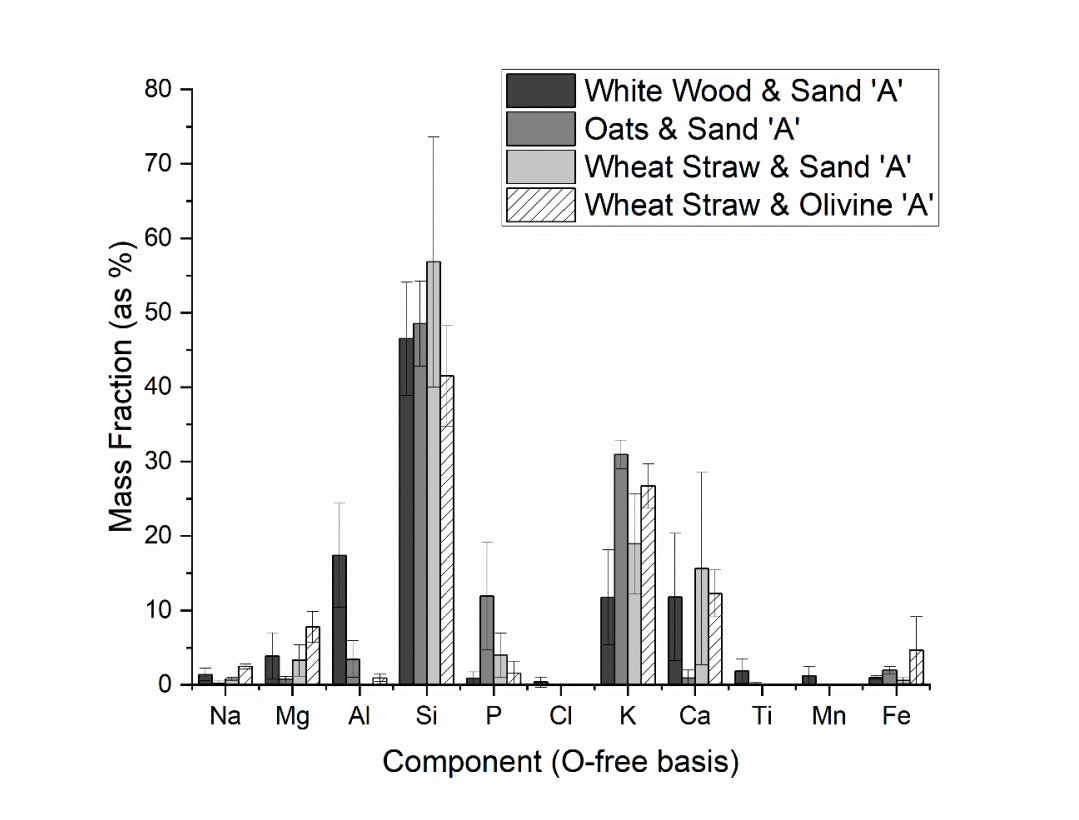

Figure 4: EDX analysis showing the effect of fuel and bed material on ash layer composition. All samples used in data averaging taken from the 'mid' vertical strata, lateral zone A, from tests at consistent operational conditions (h_{bed} 24cm, 50kWth).

When comparing ash layers when using the three fuels with sand 'A', the principal differences between the fuels are the Al, Si, P, K, and Ca content of ash layers. Aluminium content of the white wood ash deposits is high at 14%, though this is what might be expected given that white wood ash has an Al_2O_3 content of 7.5%, which is almost 5x that of the next highest fuel, wheat straw, which has a value of 1.6% (Table 1). This high aluminium content in wood ash is to be expected. Vassilev, et al. [2] analysed the composition of 86 different types of biomass, and identified an average Al_2O_3 content of wood ash to be 5.09wt.%, versus 1.39wt.% for agricultural biomass and 2.71wt.% for straws. Whilst the white wood used here has higher Al_2O_3 content than the average reported by Vassilev, et al. [2] it is far below the maximum value reported of 15.12wt.%. This elevated Al content of the white wood may be beneficial in mitigating agglomeration, as aluminosilicate additives such as kaolin are known to be effective in reducing agglomeration [20, 30]. This higher Al content may have enabled the formation of stable high melting point alkali aluminosilicate compounds (e.g.

$K_2O.Al_2O_3.nSiO_2$) [30], as opposed to formation of low melting point alkali silicates (e.g. $K_2O.nSiO_2$), which would be another contributory factor to the lack of agglomeration issues with white wood. Further study would be needed to prove the presence and formation of these compounds, however.

Both white wood and oat hull waste show similar Si contents in their ash coatings, whereas wheat straw presented notably more Si, albeit with more variance. This is likely due to silica being a more integral factor in the larger ash phases present with the melt-induced agglomerates found when using wheat straw. The higher phosphorous content of the oat hull waste ash likely assisted the propagation of agglomeration, with others having noted phosphorous to react to form high melting point calcium phosphates or low melting point potassium phosphates in prior works [34, 35, 36]. Given the low quantity of calcium in the oat hull waste ash, it is likely that there was formation of low melting point potassium phosphates in addition to reaction of potassium with silica, altering the mechanism by which agglomeration proceeds and possibly exacerbating agglomeration issues with the oat hull waste relative to its relatively low total ash content of 2.5%.

As shown in Figure 4, when using olivine 'A' with wheat straw, there is around 8% MgO in the ash melt surrounding olivine, which is more than double the 3.6% MgO present in wheat straw fuel ash itself as per Table 1. Iron content is also elevated in the ash around olivine at around 5%, versus 1% Fe_2O_3 in the wheat straw ash itself (Table 1). When considering contents of magnesium and iron in ash melts when using sand 'A' and wheat straw, it can be seen that there is around 4% magnesium and <1% iron, both of which are in line with what would be expected as per the fuel ash analysis (Table 1). Furthermore, calcium contents in ash melts around olivine are on average around 4% lower than those in ash melts with wheat straw and sand 'A' (Figure 4). This adds further qualitative support to the theory that a mechanism similar to that proposed by Kuba, et al. [29] for wood fuels and olivine has occurred here with wheat straw and olivine, as was discussed in detail in section 3.3.1. This mechanism is where calcium has migrated from ash into the crystal structure of the olivine, expelling magnesium and iron oxides from olivine into the ash, hence the elevated levels of these in the ash surrounding olivine.

3.3.3. Compositional Variation with Sampling Location

3.3.3.1. Bed Height Variation

Figure 5a shows the effect of static bed height on ash coating layer composition for white wood and oat hull waste pellets. The zone from which all samples were taken (mid vertical strata, zone A; see Figure 1 for zonal map) is a fixed location relative to the geometry of the combustion chamber. This location will therefore be lower from the bed surface with each increase to h_{bed}. There are a few consistent trends seen with increases to bed height for both white wood and oat hull waste, namely a decrease in Si and K content (albeit a very minor decrease in K for oat hull waste), and an increase in Ca content. A likely explanation for this is the effect of increases to bed height on vertical mixing within the bed. As discussed in section 3.2, bubbles will coalesce to larger sizes as they rise through a larger bed height, thereby changing the vertical mixing patterns in the bed. As fuel is fed onto the bed surface, the changes to the bed height and the resultant change to mixing regimes may reduce the amount of fresh fuel mixed in to deeper regions of the bed, with the sampling location (mid vertical strata, lateral zone A) becoming deeper relative to the bed surface with each increase to h_{bed}. This lack of fresh fuel in deeper regions of the bed would limit the amount of potassium available to attack the sand bed particle, allowing calcium silicate to form in the ash layers and displace potassium. Calcium inclusion in melt layers has been suggested by others to cause the displacement and release of potassium to the gaseous phase [54], and to protect bed particles from further ash attack [11]. The combined effects of these behaviours would therefore lead to the composition variance in K and Ca seen here.

The work of Duan, et al. [17] analysed potassium contents of agglomerates retrieved from different vertical regions of the bed when using rice straw, as well as blends with coal. They recorded that samples retrieved from higher regions of the bed had elevated potassium contents, which would agree with the observation here. A potassium delta of around 2.75wt.% was seen by Duan, et al. [17] between their grid zone region and upper bed region for tests with rice straw only, albeit with a very large relative difference (0.25wt.% in the grid zone, to 3wt.% in the upper bed region). In comparison, the largest potassium delta here was 6.7% between the two white wood cases, but with a smaller relative difference as evident from Figure 5a. Unfortunately, Duan, et al. [17]

did not analyse the prevalence of other components in agglomerates aside from potassium, therefore a broader comparison cannot be drawn.

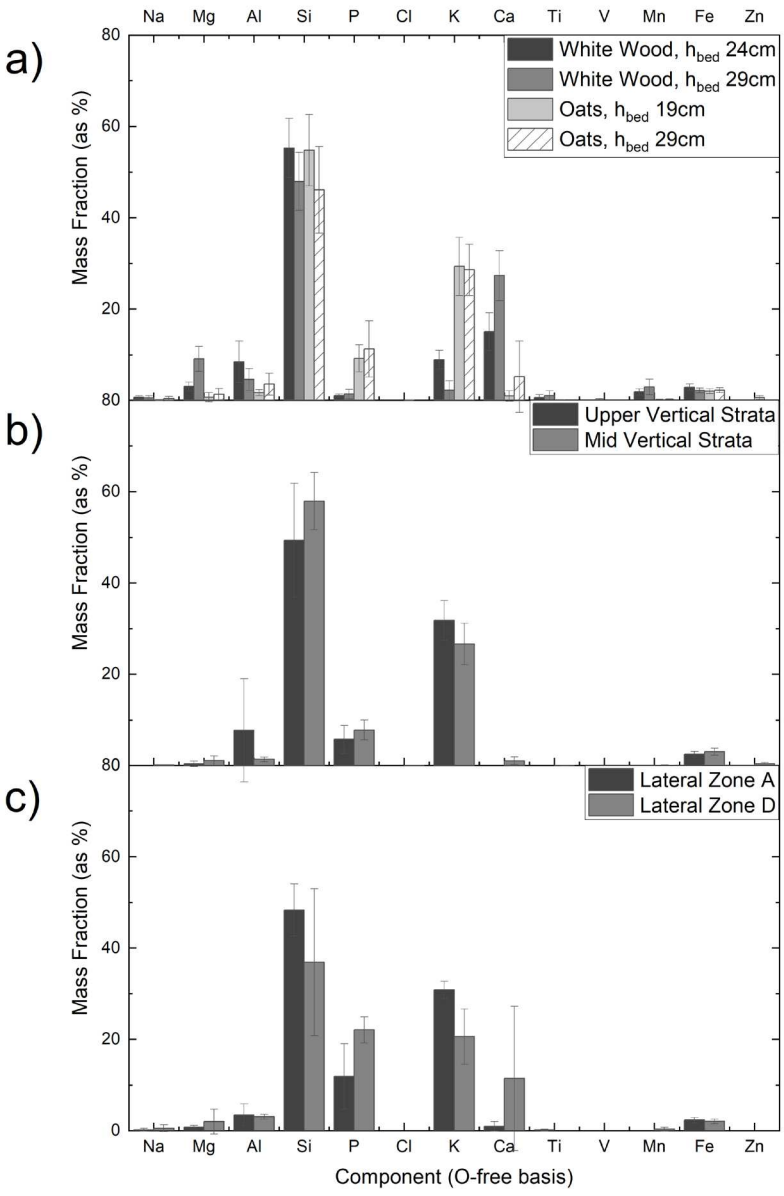

Figure 5: EDX analysis showing the effect of spatial variation within the bed on ash layer composition. a) Effect of bed height on ash layer composition. Samples taken from same test (sand 'A' at 50kWth) and location (mid vertical strata, lateral zone A). b) Effect of moving from the upper to the mid vertical strata within the bed. Test conditions: oat hull waste, sand 'A', h_{bed} 19cm, 50kWth. c) Effect of moving from lateral zone A to zone D across the mid vertical strata. Test conditions: oat hull waste, sand 'A', h_{bed} 29cm, 50kWth.

3.3.3.2. Vertical Strata Sampling

Figure 5b shows the differences in composition for agglomerate ash layers taken from different vertical zones (see Figure 1 for zonal map) of the bed, for tests using oat hull waste and sand 'A'. In comparison to samples from the upper vertical strata, samples from the mid vertical strata presented ~5% less K and ~6% less Al, and ~4% more Ca. The potassium delta seen here between the two vertical strata is again similar to that seen in section 3.3.3.1, which was 6.7%. The same trend has again been exhibited for potassium and calcium content as seen with variation to bed height (section 3.3.3.1): moving down the bed, away from the surface onto which fresh fuel is fed, bed particle ash layers have less K and more Ca. Once again the reasoning for this composition difference across vertical strata is likely similar: a reduced availability of fresh potassium in lower regions of the bed allowing for formation of more calcium silicate in the ash layers and displacement of potassium, in turn preventing further potassium reaction with the bed particle. The finding here of reduced potassium content at lower levels of the bed is again in agreement that of Duan, et al. [17] who analysed potassium content at different vertical levels of the bed for a lab-scale fluidized bed combustor. Once again, the difference in potassium content seen here is greater at ~5wt.% than that seen by Duan, et al. [17] (2.75wt.%), though the relative difference seen here is far smaller than the 12x delta seen by Duan, et al. [17].

3.3.3.3. Lateral Zone Sampling

Differences in agglomerate ash layer composition across lateral zones A and D (see Figure 1 for zonal map) of the bed were compared for oat hull waste and sand 'A', and are shown in Figure 5c. As can be seen, there are clear compositional differences between agglomerate samples from zone D, a corner away from the fuel landing location onto the bed, versus zone A where fuel approximately lands in the centre of the bed. In zone D, ash layers presented elevated amounts of phosphorous and calcium, and lower levels of silicon and potassium. Other elements were present in negligible amounts or had little to no variation between the two zones. As with bed height variation and vertical strata variation, agglomerates in zone D, further from the landing location of fuel onto the bed (zone A), had reduced K and elevated Ca in their ash coatings. Therefore, it is likely that this would be due to the same reasoning suggested previously in sections 3.3.3.1 and 3.3.3.2: zones further from the fresh fuel feed landing

location onto the bed receiving less fresh potassium, thus allowing for more development of calcium silicate in ash layers, displacement of potassium, and less attack on the bed particle surface from potassium. Unlike differences across vertical locations of the bed as briefly analysed by Duan, et al. [17], differences in agglomeration composition laterally across the bed have received no prior investigation in the literature, limiting the ability for comparison. However, it does again show that there is spatial variation to agglomeration.

These findings of spatial variance in agglomerate ash layer composition laterally and vertically across sections 3.3.3.1-3.3.3.3 would suggest that if a targeted agglomeration mitigation method were to be designed, it would be best to target location(s) in which fresh fuel initially lands on and mixes into the bed. The cross-sectional bed area of the pilot-scale fluidized bed used here is 39x35cm with a single screw feeder, whereas industrial BFB boilers often have bed cross-sectional lengths/widths upwards of several metres, with multiple screw feeders [38]. Therefore, there may be value in exploring a zonal analysis of agglomerates in a commercial BFB boiler to determine the amount of variance when moving to a larger scale with a more complex fuel feeding arrangement. This may also be of use if considering improvements to the number of fuel feeder inputs or locations within BFB boilers. A further way to expand the bed spatial analysis approach taken here would be to measure the particle size distribution of bed material retrieved from different regions of the bed. This would allow for quantification of the occurrence of agglomerates within the bed, and identification of any problematic bed regions.

4. Conclusions

This study has shown that an olivine bed material can extend defluidization time versus silica sand for fuels predisposed to melt-induced agglomeration such as wheat straw. However, it still cannot make them viable fuels overall in comparison to the likes of white wood, also tested here, which has few issues with agglomeration due to its very low ash content. With olivine and wheat straw there was the observation of a unique calcium-rich layer in ash adjacent to olivine, which has not previously been observed in the context of wheat straw combustion on an olivine bed. This behaviour may partially mitigate agglomeration due to the higher melting point of calcium silicate compounds.

It was also observed that potassium silicate in ash would migrate into cracks in olivine, likely due to capillary action, without evidence of inward reaction between potassium in ash and the bed material as has been reported by others. This would likely strengthen the agglomerate structures that do form.

EDX analysis of agglomerates from oat hull waste and silica sand tests from different bed locations showed that agglomerates retrieved from areas of the bed further away from the landing point of fuel onto the bed had reduced potassium content and elevated calcium content. It is suggested that this is due to the reduced availability of fresh fuel ash in these regions, preventing the continual attack and reaction of potassium with silica in the bed particle. This spatial variation in agglomerate composition has not previously been noted in the literature and would be worthy of further study and consideration.

5. Acknowledgements

The authors acknowledge UK EPSRC funding support through research grant no. EP/M01536X/1 and EPSRC Centre for Doctoral Training in CCS and Cleaner Fossil Energy, grant no. EP/L016362/1.

6. References

[1] E. Johnson, "Goodbye to carbon neutral: Getting biomass footprints right," *Environmental Impact Assessment Review,* vol. 29, no. 3, pp. 165-168, 2009.

[2] S. Vassilev, D. Baxter, L. Andersen and C. Vassileva, "An overview of the chemical composition of biomass," *Fuel,* vol. 89, no. 5, pp. 913-933, 2010.

[3] P. Basu, Combustion and Gasification in Fluidized Beds, 1st ed., Taylor & Francis, 2006.

[4] F. Johnsson, "Fluidized Bed Combustion for Clean Energy," Vancouver, Canada, 2007.

[5] J. DeFusco, J. McKenzie and F. M.D., "Bubbling Fluidized Bed or Stoker — Which is the Right Choice for Your Renewable Energy Project?," CIBO 20th Fluidized Bed Combustion Conference, Lexington, Kentucky, USA, 2007.

[6] A. Khan, W. de Jong, P. Jansens and H. Spliethoff, "Biomass combustion in fluidized bed boilers: Potential problems and remedies," *Fuel Processing Technology,* vol. 90, no. 1, pp. 21-50, 2009.

[7] Y. Niu, H. Tan and S. Hui, "Ash-related issues during biomass combustion: Alkali-induced slagging, silicate melt-induced slagging (ash fusion), agglomeration, corrosion, ash utilization, and related countermeasures," *Progress in Energy and Combustion Science,* vol. 52, pp. 1-61, 2016.

[8] J. Morris, S. Daood, S. Chilton and W. Nimmo, "Mechanisms and mitigation of agglomeration during fluidized bed combustion of biomass: A review," *Fuel,* vol. 230, pp. 452-473, 2018.

[9] H. Visser, "The Influence of Fuel Composition on Agglomeration Behaviour in Fluidised-Bed Combustion," Energy Research Centre of the Netherlands (ECN), 2004.

[10] E. Brus, M. Öhman and A. Nordin, "Mechanisms of Bed Agglomeration during Fluidized-Bed Combustion of Biomass Fuels," *Energy & Fuels,* vol. 19, no. 3, pp. 825-832, 2005.

[11] H. He, D. Boström and M. Öhman, "Time Dependence of Bed Particle Layer Formation in Fluidized Quartz Bed Combustion of Wood-Derived Fuels," *Energy & Fuels,* vol. 28, no. 6, pp. 3841-3848, 2014.

[12] F. Scala and R. Chirone, "Characterization and Early Detection of Bed Agglomeration during the Fluidized Bed Combustion of Olive Husk," *Energy & Fuels,* vol. 20, no. 1, pp. 120-132, 2006.

[13] A. Malmgren and G. Riley, "Biomass Power Generation," in *Comprehensive*

Renewable Energy, A. Sayigh, Ed., Elsevier, 2012, pp. 27-53.

[14] M. Öhman, A. Nordin, B.-G. Skrifvars, R. Backman and M. Hupa, "Bed Agglomeration Characteristics during Fluidized Bed Combustion of Biomass Fuels," *Energy & Fuels,* vol. 14, no. 1, pp. 169-178, 2000.

[15] M. Öhman, L. Pommer and A. Nordin, "Bed Agglomeration Characteristics and Mechanisms during Gasification and Combustion of Biomass Fuels," *Energy & Fuels,* vol. 19, no. 4, pp. 1742-1748, 2005.

[16] C. Yu, J. Qin, H. Nie, M. Fang and Z. Luo, "Experimental research on agglomeration in straw-fired fluidized beds," *Applied Energy,* vol. 88, no. 12, pp. 4534-4543, 2011.

[17] F. Duan, C.-S. Chyang, L.-H. Zhang and S.-F. Yin, "Bed agglomeration characteristics of rice straw combustion in a vortexing fluidized-bed combustor," *Bioresource Technology,* vol. 183, pp. 195-202, 2015.

[18] W. Lin, K. Dam-Johansen and F. Frandsen, "Agglomeration in bio-fuel fired fluidized bed combustors," *Chemical Engineering Journal,* vol. 96, no. 1-3, pp. 171-185, 2003.

[19] H. Liu, Y. Feng, S. Wu and D. Liu, "The role of ash particles in the bed agglomeration during the fluidized bed combustion of rice straw," *Bioresource Technology,* vol. 100, no. 24, pp. 6505-6513, 2009.

[20] E. Zabetta, V. Barišić, K. Peltola and A. Hotta, "Foster Wheeler Experience with biomass and waste in CFBs," in *33rd International Technical Conference on Coal Utilization and Fuel Systems*, Clearwater, Florida, 2008.

[21] C. Atkinson, "Establishing perennial grass energy crops in the UK: A review of current propagation options for Miscanthus," *Biomass and Bioenergy,* vol. 33, no. 5, pp. 752-759, 2009.

[22] J. Kaknics, R. Michel, A. Richard and J. Poirier, "High-Temperature Interactions between Molten Miscanthus Ashes and Bed Materials in a Fluidized-Bed Gasifier," *Energy & Fuels,* vol. 29, no. 3, pp. 1785-1792, 2015.

[23] H. Chi, M. Pans, C. Sun and H. Liu, "An investigation of lime addition to fuel as a countermeasure to bed agglomeration for the combustion of non-woody biomass fuels in a 20kWth bubbling fluidised bed combustor," *Fuel,* vol. 240, pp. 349-361, 2019.

[24] R. Michel, J. Kaknics, E. de Bilbao and J. Poirier, "The mechanism of agglomeration of the refractory materials in a fluidized-bed reactor," *Ceramics International,* vol. 42, no. 2, pp. 2570-2581, 2016.

[25] M. Bartels, W. Lin, J. Nijenhuis, F. Kapteijn and J. van Ommen, "Agglomeration in fluidized beds at high temperatures: Mechanisms, detection and prevention," *Progress in Energy and Combustion Science,* vol. 34, no. 5, pp. 633-666, 2008.

[26] A. Grimm, M. Öhman, T. Lindberg, A. Fredriksson and D. Boström, "Bed

Agglomeration Characteristics in Fluidized-Bed Combustion of Biomass Fuels Using Olivine as Bed Material," *Energy & Fuels,* vol. 26, no. 7, pp. 4550-4559, 2012.

[27] F. Kirnbauer and H. Hofbauer, "Investigations on Bed Material Changes in a Dual Fluidized Bed Steam Gasification Plant in Güssing, Austria," *Energy & Fuels,* vol. 25, no. 8, pp. 3793-3798, 2011.

[28] F. Kirnbauer and H. Hofbauer, "The mechanism of bed material coating in dual fluidized bed biomass steam gasification plants and its impact on plant optimization," *Powder Technology,* vol. 245, pp. 94-104, 2013.

[29] M. Kuba, H. He, F. Kirnbauer, N. Skoglund, D. Boström, M. Öhman and H. Hofbauer, "Mechanism of Layer Formation on Olivine Bed Particles in Industrial-Scale Dual Fluid Bed Gasification of Wood," *Energy & Fuels,* vol. 30, no. 9, pp. 7410-7418, 2016.

[30] L. Wang, J. Hustad, Ø. Skreiberg, G. Skjevrak and M. Grønli, "A Critical Review on Additives to Reduce Ash Related Operation Problems in Biomass Combustion Applications," *Energy Procedia,* vol. 20, pp. 20-29, 2012.

[31] K. Davidsson, L. Åmand, B. Steenari, A. Elled, D. Eskilsson and B. Leckner, "Countermeasures against alkali-related problems during combustion of biomass in a circulating fluidized bed boiler," *Chemical Engineering Science,* vol. 63, no. 21, pp. 5314-5329, 2008.

[32] C. Lin and M. Wey, "The effect of mineral compositions of waste and operating conditions on particle agglomeration/defluidization during incineration," *Fuel,* vol. 83, no. 17-18, pp. 2335-2343, 2004.

[33] P. Chaivatamaset, P. Sricharoon and S. Tia, "Bed agglomeration characteristics of palm shell and corncob combustion in fluidized bed," *Applied Thermal Engineering,* vol. 31, no. 14-15, pp. 2916-2927, 2011.

[34] V. Barišić, L.-E. Åmand and E. Zabetta, "The role of limestone in preventing agglomeration and slagging during CFB combustion of high-phosphorous fuels," in *World Bioenergy 2008*, Jönköping, Sweden, 2008.

[35] A. Grimm, N. Skoglund, D. Boström and M. Öhman, "Bed Agglomeration Characteristics in Fluidized Quartz Bed Combustion of Phosphorus-Rich Biomass Fuels," *Enery & Fuels,* vol. 25, no. 3, pp. 937-947, 2011.

[36] P. Billen, B. Creemers, J. Costa, J. Van Caneghem and C. Vandecasteele, "Coating and melt induced agglomeration in a poultry litter fired fluidized bed combustor," *Biomass and Bioenergy,* vol. 69, pp. 71-79, 2014.

[37] P. Xing, P. Mason, S. Chilton, S. Lloyd, J. Jones, A. Williams, W. Nimmo and M. Pourkashanian, "A comparative assessment of biomass ash preparation methods using X-ray fluorescence and wet chemical analysis," *Fuel,* vol. 182, pp. 161-165, 2016.

[38] B. Leckner, P. Szentannai and F. Winter, "Scale-up of fluidized-bed combustion –

A review," *Fuel,* vol. 90, no. 10, pp. 2951-2964, 2011.

[39] F. Scala and R. Chirone, "An SEM/EDX study of bed agglomerates formed during fluidized bed combustion of three biomass fuels," *Biomass and Bioenergy,* vol. 32, no. 3, pp. 252-266, 2008.

[40] J. Goldstein, D. Newbury, D. Joy, C. Lyman, P. Echlin, E. Lifshin, L. Sawyer and J. Michael, Scanning Electron Microscopy and X-Ray Microanalysis, 3rd Edition, New York: Springer, 2003.

[41] B. Gatternig and J. Karl, "Investigations on the Mechanisms of Ash-Induced Agglomeration in Fluidized-Bed Combustion of Biomass," *Energy & Fuels,* vol. 29, pp. 931-941, 2015.

[42] M. Huttunen, J. Peltola, S. Kallio, L. Karvonen, T. Niemi and V. Ylä-Outinen, "Analysis of the processes in fluidized bed boiler furnaces during load changes," *Energy Procedia,* vol. 120, pp. 580-587, 2017.

[43] J. Ribeiro, E. Vicente, C. Alves, X. Querol, F. Amato and L. Tarelho, "Characteristics of ash and particle emissions during bubbling fluidised bed combustion of three types of residual forest biomass," *Environmental Science and Pollution Research,* vol. 24, no. 11, pp. 10018-10029, 2017.

[44] G. Olofsson, W. Wang, Z. Ye, I. Bjerle and A. Andersson, "Repressing NOx and N2O Emissions in a Fluidized Bed Biomass Combustor," *Energy & Fuels,* vol. 16, no. 4, pp. 915-919, 2002.

[45] A. Keppel, J. Finnan, B. Rice, P. Owende and K. MacDonnell, "Cereal grain combustion in domestic boilers," *Biosystems Engineering,* vol. 115, no. 2, pp. 136-143, 2013.

[46] European Parliament, *Directive 2010/75/EU of the European Parliament and of the Council on Industrial Emissions,* Brussels, Belgium: European Union, 2010.

[47] E. Zabetta, M. Hupa and K. Saviharju, "Reducing NOx Emissions Using Fuel Staging, Air Staging, and Selective Noncatalytic Reduction in Synergy," *Industrial & Engineering Chemistry,* vol. 44, no. 13, pp. 4552-4561, 2005.

[48] F. Sher, M. Pans, D. Afilaka, C. Sun and H. Liu, "Experimental investigation of woody and non-woody biomass combustion in a bubbling fluidised bed combustor focusing on gaseous emissions and temperature profiles," *Energy,* vol. 141, pp. 2069-2080, 2017.

[49] J. Meng, X. Wang, Z. Zhao, A. Zheng, Z. Huang, G. Wei, K. Lv and H. Li, "Highly abrasion resistant thermally fused olivine as in-situ catalysts for tar reduction in a circulating fluidized bed biomass gasifier," *Bioresource Technology,* vol. 268, pp. 212-220, 2018.

[50] R. Beetstra, J. Nijenhuis, N. Ellis and J. van Ommen, "The influence of the particle size distribution on fluidized bed hydrodynamics using high-throughput experimentation," *AIChE Journal,* vol. 55, no. 8, pp. 2013-2023, 2009.

[51] L. Shartsis and S. Spinner, “Surface tension of molten alkali silicates,” *Journal of Research of the National Bureau of Standards,* vol. 46, no. 5, pp. 385-390, 1951.

[52] S. Sharma and W. Philbrook, “Improved Values of Surface Tension of Calcium Silicate Melts,” *Scripta Metallurgica,* vol. 4, no. 2, pp. 107-109, 1970.

[53] A. Elled, L. Åmand and B. Steenari, “Composition of agglomerates in fluidized bed reactors for thermochemical conversion of biomass and waste fuels,” *Fuel,* vol. 111, pp. 696-708, 2013.

[54] P. Thy, C. Lesher and B. Jenkins, “Experimental determination of high-temperature elemental losses from biomass slag,” *Fuel,* vol. 79, pp. 693-700, 2000.

Supplementary Data

Agglomeration and the effect of process conditions on fluidized bed combustion of biomasses with olivine and silica sand as bed materials: Pilot-scale investigation

Jonathan D. Morris[a], Syed Sheraz Daood[a,b,*], William Nimmo[a]

[a] *Energy Engineering Group, Energy 2050, Department of Mechanical Engineering, University of Sheffield, Sheffield, S3 7RD, United Kingdom*

[b] *Institute of Chemical Engineering and Technology, University of the Punjab, Quaid-e-Azam Campus, Lahore, Pakistan*

** Corresponding author at: Ella Armitage Building, Energy Engineering Group, Energy 2050, Department of Mechanical Engineering, University of Sheffield, Sheffield, S3 7RD, UK.*

E-mail addresses: s.daood@sheffield.ac.uk; sdaood.icet@pu.edu.pk (S.S. Daood); w.nimmo@sheffield.ac.uk (W. Nimmo)

1. Example: Lost Revenue Due to Bed Defluidization Outage

This supplementary data file contains a simplified example calculation of lost revenues arising from an unplanned boiler outage caused by a bed defluidization event. This is for an example biomass combined heat & power (CHP) fluidized bed boiler in the UK.

Table 1: Example calculation for lost revenues due to unplanned boiler outage.

Assumed Boiler Conditions & Pricing	
Boiler Thermal Input	100MWth
Turbine Electrical Power Output	35MWe
Electricity Wholesale Price[1]	£40 per MWh[1]
Renewable Obligation Certificates (ROCs) awarded per MWh of generation[2]	2.0[2, p. 12]
Value of each ROC awarded	£45 per ROC[1]
Revenue per hour of generation (electrical generation only)	£4,550
Downtime & Lost Revenue Calculation	
Downtime: Boiler Cooldown[3]	36 hours
Downtime: Bed Removal/Cleaning & Inspection Team[4]	8 hours
Start-up & Return to Load[5]	8 hours
Total Lost Revenue Period	52 hours
Total Lost Revenue[6]	£236,600

[1] Example day-ahead electrical wholesale price for January 2020.

[2] Biomass CHP plants are awarded 2.0 ROCs per MWh in the UK if they operate under the Renewable Obligation scheme. This is assuming that they reach a quality index (QI) value of 100 under the UK's Combined Heat & Power Quality Assurance Scheme (CHPQA).

[3] Assuming some degree forced cooling of boiler with air.

[4] Removal of the bed material not drained by ash chutes, and some removal of slag on bed refractory regions/air grid where needed.

[5] Some revenue generation would occur during start-up but assumed as £0 for purposes of calculation.

[6] This lost revenue calculation does not consider the value of lost heat exports as part of CHP. The value of this may vary substantially depending on contracts and penalties. In addition, as this calculation is a simplified calculation of lost revenues only, a variety of other factors will impact the net cost of an unplanned outage, including but not limited to: standing costs (e.g. staffing), cost of additional bed replacement/disposal, savings on unburnt fuel, any penalties incurred due to supply contracts, etc. Downtime and start-up times quoted above serve as examples, and may vary depending on boiler size, technology, heating/cooling rate limitations, additional remedial works required, etc.

2. References

[1] Ofgem, “Wholesale Market Indicators,” Ofgem, 2020. [Online]. Available: https://www.ofgem.gov.uk/data-portal/wholesale-market-indicators. [Accessed 21 January 2020].

[2] Department for Business, Energy and Industrial Strategy, “Simple Guide to the CHP Quality Assurance (CHPQA) Programme,” UK Government, London, 2019.

[3] Waste & Resources Action Programme (WRAP), “Market Situation Report - Summer 2011: Realising the value of recovered wood,” 2011. [Online]. Available: http://www.wrap.org.uk/sites/files/wrap/Wood%20Market%20Situation%20Report_0.pdf. [Accessed 21 January 2020].